Eur. Phys. J. Special Topics **228**, 2511–2530 (2019)

https://doi.org/10.1140/epjst/e2019-900074-1

THE EUROPEAN PHYSICAL JOURNAL SPECIAL TOPICS

Regular Article

# A study of Rayleigh–Bénard convection in hybrid nanoliquids with physically realistic boundaries

C. Kanchana[1,2], P.G. Siddheshwar[3], and Yi Zhao[1,2,a]

[1] GuiZhou University, State Laboratory of Public Big Data, Guizhou, Guiyang 550025, P.R. China
[2] College of Science, Harbin Institute of Technology, Shenzhen, University Town, Nanshan District, Guangdong Province, Shenzhen-518055, P.R. China
[3] Department of Mathematics, Bangalore University, Jnanabharathi Campus, Bangalore 560056, India

Received 22 April 2019 / Received in final form 6 June 2019
Published online 6 December 2019

**Abstract.** Linear and weakly nonlinear stability analyses of Rayleigh–Bénard convection in water–copper–alumina hybrid nanoliquid bounded by rigid isothermal boundaries is studied analytically. A single-phase description is used for the nanoliquid. Using a minimal Fourier series representation and an appropriate scaling a classical Lorenz model for rigid isothermal boundaries is derived. The Lorenz model is transformed to the Ginzburg–Landau model using the renormalization group method. The solution of the Ginzburg–Landau model is used to arrive at the expression of the Nusselt number. The study shows that the presence of two nanoparticles in water is to increase the coefficient of friction, advance the onset of convection and enhance the heat transfer. Further, it is shown that compared to a single nanoparticle the combined influence of two nanoparticles is more effective on heat transfer. The percentage of heat transfer enhancement in water due to $Al_2O_3-Cu$ hybrid nanoparticles is almost twice that of $Al_2O_3$ nanopartcles. It is found that the hybrid nanoparticles of $Al_2O_3-Cu$ intensify convection in water more than the mono nanoparticles of $Al_2O_3$ and the plots of stream function and isotherm point to this fact. The effect of the physically realistic rigid boundaries is to inhibit the onset of convection when compared with that of free boundaries.

## 1 Introduction

In early days of technological advancement, heat removal in many electrical, electronic and mechanical devices was achieved by using the abundantly available coolants like air and water. Later liquids like oil and ethylene glycol were used. Attempts at enhancement of heat transfer in fluid media continued and have been going on for several decades (see [1,2] and references therein). Alterations to the geometry was first made to achieve this objective of efficient cooling. Fins, windows, exhausts and other

[a] e-mail: zhao.yi@hit.edu.cn

**Table 1.** Common choice of base liquid and nanoparticles/nanotubes [10]–[15].

| Type | Material |
|---|---|
| Base liquid | Water, ethylene glycol, methanol, engine oil, glycerine |
| Metal | Diamond, gold, silver, copper, aluminum, silicon, titanium, zinc |
| Metal oxide | Copper oxide, alumina, silica, titania |
| Nanotube | Single-walled carbon nanotubes, double-walled carbon nanotubes, multi-walled carbon nanotubes, functional carbon nanotubes |

ideas were implemented and put to great use in application situations (see [3,4] and references therein). Subsequently researchers came up with the idea of introducing micron-sized particles of higher thermal conductivity compared with that of the base liquid they were dispersed in. This turned out to be an impractical proposition since fluid systems where this idea was implemented suffered from pressure loss, clogging and wall destruction. Stability of the micron-sized particles in the base liquid was also an issue. With sophistication in manufacturing technology miniaturisation of the devices was a natural consequence and micron-sized particles could not be a viable solution. This lead people to go in for much smaller sized particles than the micron-sized ones. With success in the synthesis of nanoparticles and also with the understanding that the main thermophysical property of thermal conductivity gets enhanced due to the reduction in size (see [5]), quite naturally researchers restarted heat transfer research using this exciting new prospect of well-dispersed nanoparticles in a coolant (see [6–8] and references therein). The very small size of the nanoparticles meant that they were nearly the size of the fluid particles and hence fluidity was not compromised much by the introduction of these. Most importantly fluid systems with nanoparticles did not suffer from the deficiencies suffered by them on using micron-sized particles(see [9]). With this new finding, experimentation was made trying out different nanoparticles of different materials – metallic and non-metallic ones, oxides, and others. Some of the nanoparticles and base liquids used are listed in Table 1.

The nanoparticles of same material and spherical shape was well-dispersed in a noncarcinogenic base fluid and was termed as 'nanofluid' by Choi [7]. Innumerable laboratory experiments then followed in trying out appropriate nanofluids for various heat transfer applications. The thermal conductivity enhancement due to addition of a dilute concentration of nanoparticles was first reported by Masuda et al. [6] who showed that dilute concentration (5%) of alumina, silica and titania nanoparticles in water yield 10%–50% improvement in the thermal conductivity of water. Mintsa et al. [16] reported a thermal conductivity-temperature-nanoliquid volume fraction relation found from experiment.

Many theoretical models were developed to study the stability and the heat transfer performance of nanofluids. These models are based on either the single-phase (where base liquid particles and nanoparticles are indistinguishable) or the two-phase description. Buongiorno [17] argued in favor of two-phase model and he developed a transport equation to study the nanoparticle concentration in the flow model. Siddheshwar et al. [18] generalized Buongiorno two-phase model by incorporating thermophysical properties of nanoliquids. Siddheshwar and Lakshmi [19] extended the generalized Buongiorno model to include a porous medium. Garoosi et al. [20] reported that at high Rayleigh number the single-phase model proposed by Khanafer et al. [21] is good enough to predict the stability of convection and heat transport in nanoliquids. Jou and Tzeng [22] presented an empirical relation between the average Nusselt number and the volume fraction of nanoparticles. Siddheshwar and Meenakshi [23] reported the heat transfer enhancement in four base liquids for

twenty nanoparticles. Simo et al. [24], Jawdat et al. [25] and Kanchana et al. [13] studied chaotic convective motion in a nanoliquid layer heated from below.

In the quest for future coolants with much higher thermal conductivity than that of nanofluids, researchers considered a base fluid well-dispersed with two or more types of nanoparticles (see [26–34]). Further, some of the researchers considered two well-mixed base liquids and introduced one or more type of nanoparticles and experimented with them [35]. Such nanofluids were called as 'hybrid nanofluids'. These can also be termed 'nanocomposite fluids' or even 'new generation nanofluids'. An important finding of the research conducted on all types of nanofluids is that only dilute concentration of nanoparticles will have to be used in the base liquid in order to avoid agglomeration and retain large surface area of heat transfer in each nanoparticle. A recent finding concerns some hybrid nanofluids that showed 'enhanced heat transfer' when compared with that of nanofluids with one type of nanoparticle [28].

At the present time experimentation is still on to try out different nanofluids and hybrid nanofluids and thus this paper must only be viewed as a small theoretical endeavor in the direction of moving from TRL (Technology Readiness Level) 4 (laboratory experiments) to TRL 5 (actual applications). In the world today search for future coolants is an ongoing process and the synergising factor of nanoparticles in the case of hybrid nanofluids is an important aspect to be researched. Findings in one type of heat transfer problem may throw light on another type of heat transfer application and hence in this spirit we present this study of Rayleigh–Bénard convection in hybrid nanofluids and a representative one, viz., water-copper-alumina is chosen for investigation. Unlike in the case of single nanoparticle in base liquid where we can find many models to study the thermal conductivity and the viscosity of nanoliquids, in the case of hybrid nanoliquid there is no such model. Hence, we have used the experimental data reported by Suresh et al. [26] for thermal conductivity and viscosity of water-cu-alumina hybrid nanoliquid. In order to compare the heat transfer performance of hybrid nanoliquids with nanoliquids we have also considered the experimental data of Suresh et al.[26] for water-alumina nanoliquid. The main objective of the paper is to contribute in a small way towards developing energy-efficient systems that have higher energy efficiency, better performance and lower operating costs.

## 2 Mathematical formulation

We consider a Rayleigh–Bénard convective system consisting of two infinite-horizontal-extent parallel plates with distance $h$ apart. The upper and lower plates are maintained at temperatures $T_0$ and $T_0 + \Delta T$ ($\Delta T > 0$) respectively as shown in Figure 1. Water–copper–alumina nanoliquid is chosen as the working medium. The instability in the system sets in as longitudinal rolls (cross-section is a circle in the $xz$-plane). The axis of these parallel rolls is along the $y-$ direction and hence a two-dimensional study in the $xz$-plane suffices. In one wavelength we can notice two rolls of which one turns clockwise and the other anticlockwise.

The following equations govern the Rayleigh–Bénard convective flow:

$$\nabla \cdot \mathbf{q} = 0, \tag{1}$$

$$\rho_{hnl} \frac{\partial \mathbf{q}}{\partial t} = -\nabla p + \mu_{hnl} \nabla^2 \mathbf{q} + \left[\rho_{hnl} - (\rho\beta)_{hnl} (T - T_0)\right] \mathbf{g}, \tag{2}$$

$$\frac{\partial T}{\partial t} + (\mathbf{q} \cdot \nabla) T = \alpha_{hnl} \nabla^2 T. \tag{3}$$

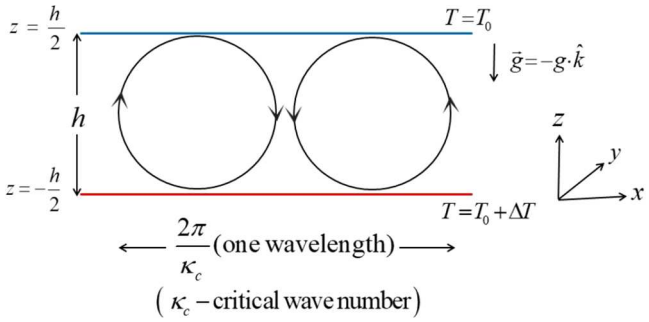


**Fig. 1.** Schematic of the Rayleigh–Bénard convection problem.

**Table 2.** Thermophysical properties of water-$Al_2O_3$−Cu nanoliquid at $T = 300$ K.

| $\phi_{hnp}$ % | $\phi_{A_2O_3}$ % | $\phi_{Cu}$ % | $k_{hnl}$ W/[m K] | $\mu_{hnl}$ kg/m s | $\rho_{hnl}$ kg/m$^3$ | $C_{p_{hnl}}$ J/kg K | $\alpha_{hnl} \times 10^7$ m$^2$/s | $\beta_{hnl} \times 10^5$ 1/K |
|---|---|---|---|---|---|---|---|---|
| 0.10 | 0.0962 | 0.0038 | 0.619982 | 0.000972 | 1000.26 | 4164.68 | 1.48828 | 20.92 |
| 0.33 | 0.3175 | 0.0125 | 0.630980 | 0.001098 | 1007.53 | 4132.08 | 1.51561 | 20.73 |
| 0.75 | 0.7215 | 0.0285 | 0.649004 | 0.001386 | 1020.81 | 4073.74 | 1.56066 | 20.39 |
| 1.00 | 0.9620 | 0.0380 | 0.657008 | 0.001602 | 1028.71 | 4039.73 | 1.58097 | 20.19 |
| 2.00 | 1.9241 | 0.0759 | 0.684992 | 0.001935 | 1060.32 | 3908.79 | 1.65274 | 19.42 |

Equations (1)–(3) are respectively continuity, momentum and energy equations. The quantities in the governing equations are $\mathbf{q} = (u, w)$, two-dimensional velocity vector with components, $u$ and $w$ in the $i$th and $k$th directions (in m), $T$ is the temperature of the hybrid nanofluid (in $K$), $\mathbf{g} = -g\hat{k}$ is the gravity (in m/s$^2$), $p$ is the pressure (in $Pa$), $\rho_{hnl}, \mu_{hnl}$ and $\beta_{hnl}$ are respectively the density, the dynamic viscosity and the thermal expansion coefficient of water-$Al_2O_3$−Cu nanoliquid (in kg/m$^3$, kg/ms and K$^{-1}$ respectively). Further, $\alpha_{hnl} = \dfrac{k_{hnl}}{C_{p_{hnl}}\rho_{hnl}}$ denotes thermal diffusivity of water-$Al_2O_3$−Cu nanoliquid (in m$^2$/s) with $k_{hnl}$ and $C_{p_{hnl}}$ being thermal conductivity and specific heat of water-$Al_2O_3$−Cu nanoliquid (in W/mK and J/kg K, respectively). These thermophysical properties vary with volume fraction of nanoparticles and temperature. In Tables 2 and 3 we have documented the thermophysical values of water-$Al_2O_3$−Cu and water-$Al_2O_3$ nanoliquid for different values of volume fraction of nanoparticles at temperature 300 K. The maximum volume fraction chosen is 2% (in the case of $Al_2O_3$−Cu it is 1.9241% of $Al_2O_3$ and 0.0759% of $Cu$) with the intention of retaining the stability of the system (see [26]). The thermal conductivity and the dynamic viscosity of water-$Al_2O_3$−Cu and water-$Al_2O_3$ nanoliquids mentioned in the Tables 2 and 3 are obtained experimentally at 300 K (see [26]). Other thermophysical properties of nanoliquids are obtained by using the thermophysical properties of water, Cu and $Al_2O_3$ (documented in Tab. 4) and the traditional mixture theory:

$$\left.\begin{aligned} \rho_{hnl} &= (1-\phi_{hnp})\,\rho_w + \phi_{\mathrm{Al_2O_3}}\,\rho_{\mathrm{Al_2O_3}} + \phi_{\mathrm{Cu}}\,\rho_{\mathrm{Cu}} \\ (\rho\beta)_{hnl} &= (1-\phi_{hnp})\,\rho_w\,\beta_w + \phi_{\mathrm{A_2O_3}}\,\rho_{\mathrm{Al_2O_3}}\,\beta_{\mathrm{Al_2O_3}} + \phi_{\mathrm{Cu}}\,\rho_{\mathrm{Cu}}\,\beta_{\mathrm{Cu}} \\ (\rho C_p)_{hnl} &= (1-\phi_{hnp})\,\rho_w\,C_{p_w} + \phi_{\mathrm{A_2O_3}}\,\rho_{\mathrm{Al_2O_3}}\,C_{p_{\mathrm{Al_2O_3}}} + \phi_{\mathrm{Cu}}\,\rho_{\mathrm{Cu}}\,C_{p_{\mathrm{Cu}}} \end{aligned}\right\}. \quad (4)$$

**Table 3.** Thermophysical properties of water-$Al_2O_3$ nanoliquid at $T = 300\,\mathrm{K}$.

| $\phi_{np}$ % | $k_{nl}$ W/[m K] | $\mu_{nl}$ kg/m s | $\rho_{0_{nl}}$ kg/m$^3$ | $C_{p_{nl}}$ J/kg K | $\alpha_{nl} \times 10^7$ m$^2$/s | $\beta_{nl} \times 10^5$ 1/K |
|---|---|---|---|---|---|---|
| 0.10 | 0.614055 | 0.000904 | 1000.07 | 4165.45 | 1.47406 | 20.92 |
| 0.33 | 0.619004 | 0.000905 | 1006.91 | 4134.58 | 1.48686 | 20.73 |
| 0.75 | 0.63098 | 0.000910 | 1019.40 | 4079.28 | 1.51736 | 20.41 |
| 1.00 | 0.64375 | 0.000952 | 1026.83 | 4047.01 | 1.54912 | 20.22 |
| 2.00 | 0.657192 | 0.000972 | 1056.56 | 3922.44 | 1.58578 | 19.49 |

**Table 4.** Thermophysical properties of water, Cu and $Al_2O_3$ at $T = 300\,\mathrm{K}$.

| Properties | $k$ W/[m K] | $\mu$ kg/m s | $\rho$ kg/m$^3$ | $C_p$ J/kg K | $\alpha \times 10^7$ m$^2$/s | $\beta \times 10^5$ 1/K |
|---|---|---|---|---|---|---|
| Water | 0.611 | 0.0009 | 997.1 | 4179 | 1.46632 | 21 |
| Cu | 401 | – | 8933 | 385 | 1163.1 | 1.67 |
| $Al_2O_3$ | 40 | – | 3970 | 765 | 131.7 | 0.85 |

Equations (1)–(3) for the dynamic state are subjected to rigid and isothermal boundary condition:

$$\left.\begin{aligned}(u,w) = (0,0),\ \frac{\partial u}{\partial x} = 0,\ \frac{\partial w}{\partial z} = 0,\ T = T_0 + \Delta T \text{ at } z = -\frac{h}{2}\\ (u,w) = (0,0),\ \frac{\partial u}{\partial x} = 0,\ \frac{\partial w}{\partial z} = 0,\ T = T_0 \text{ at } z = \frac{h}{2}\end{aligned}\right\}. \tag{5}$$

The basic state quantities are:

$$\mathbf{q}_b(z) = (0,0),\ p = p_b(z) \text{ and } T_b = T_b(z). \tag{6}$$

The solution of the basic-state temperature that significantly influences the dynamics is given by:

$$T_b(z) = T_0 + \Delta T\left(\frac{1}{2} - \frac{z}{h}\right). \tag{7}$$

Superimposing perturbations, $\mathbf{q}'(x,z,t)$, $T'(x,z,t)$ and $p'(x,z,t)$ on the basic state and using the basic state solution, we get

$$\rho_{hnl}\frac{\partial u'}{\partial t} = -\frac{\partial p'}{\partial x} + \mu_{hnl}\nabla^2 u', \tag{8}$$

$$\rho_{hnl}\frac{\partial w'}{\partial t} = -\frac{\partial p'}{\partial z} + \mu_{hnl}\nabla^2 w' - (\rho\beta)_{hnl}T'g, \tag{9}$$

$$\frac{\partial T'}{\partial t} = \alpha_{hnl}\nabla^2 T' + \frac{\Delta T}{h}w' - \left(u'\frac{\partial T'}{\partial x} + w'\frac{\partial T'}{\partial z}\right). \tag{10}$$

Differentiating equation (8) with respect to $z$ and equation (9) with respect to $x$ and subtracting these two equations, then differentiating the resultant equation with respect to $x$ again and using the continuity equation, we get

$$\rho_{hnl}\frac{\partial}{\partial t}(\nabla^2 w') = \mu_{hnl}\nabla^4 w' - (\rho\beta)_{nl}\frac{\partial^2 T'}{\partial x^2}g. \tag{11}$$

Non-dimensionalizing the equations (10) and (11) using the following definition:

$$(X, Z) = \left(\frac{x}{h}, \frac{z}{h}\right), \quad \tau = \frac{\alpha_{bl}}{h^2}t, \quad U = \frac{hu'}{\alpha_{bl}}, \quad W = \frac{hw'}{\alpha_{bl}}, \quad \Theta = \frac{T'}{\Delta T}, \tag{12}$$

we obtain the dimensionless form of the vorticity and the heat transport equations as follows:

$$\frac{\partial}{\partial \tau}\left(\nabla^2 W\right) = Pr_{hnl}\left(a_1 \nabla^4 W - a_1^2 Ra_{hnl}\frac{\partial^2 \Theta}{\partial X^2}\right), \tag{13}$$

$$\frac{\partial \Theta}{\partial \tau} = W + a_1 \nabla^2 \Theta - \left(U\frac{\partial \Theta}{\partial X} + W\frac{\partial \Theta}{\partial Z}\right), \tag{14}$$

where

$$\left.\begin{aligned} Pr_{hnl} &= \frac{\mu_{hnl}}{\rho_{hnl}\alpha_{hnl}}(\text{hybrid nanoliquid Prandtl number}) \\ Ra_{hnl} &= \frac{(\rho\beta)_{hnl}\, g\Delta T\, h^3}{\alpha_{hnl}\mu_{hnl}}(\text{hybrid nanoliquid Rayleigh number}) \\ a_1 &= \frac{\alpha_{hnl}}{\alpha_{bl}}(\text{ diffusivity ratio}) \end{aligned}\right\}. \tag{15}$$

We note here that $a_1$ is an important parameter in hybrid nanoliquids. We show later on that $a_1$ is essentially the relative coefficient of friction.

The boundary condition (5) as considered for the dynamic state is:

$$W = \frac{\partial W}{\partial Z} = \Theta = 0 \quad \texttt{at} \quad Z = \pm\frac{1}{2}. \tag{16}$$

In the next subsection we derive the classical Lorenz model for rigid boundaries using the minimal Fourier–Galerkin expansion.

### 2.1 Derivation of the classical Lorenz model for rigid boundaries

The minimal (normal) Fourier–Galerkin expansion to study the Rayleigh–Bénard convection in water-$Al_2O_3$−Cu hybrid nanoliquids bounded by rigid isothermal boundaries is:

$$U(X, Z, \tau) = -\frac{\sqrt{2}\delta^2 a_1}{\pi\kappa_c} m_1 A(\tau) f_1(X, Z), \tag{17}$$

$$W(X, Z, \tau) = \frac{\sqrt{2}\delta^2 a_1}{\pi} m_1 A(\tau) f_2(X, Z), \tag{18}$$

$$\Theta(X, Z, \tau) = \frac{1}{\pi r_{hnl}}\left[\sqrt{2} m_2 B(\tau) f_3(X, Z) - m_3 C(\tau) f_4(Z)\right], \tag{19}$$

where $m_1$, $m_2$ and $m_3$ are chosen in such a way that we are led to the Lorenz model for rigid boundaries in classical form. These $m_i$'s are chosen as follows:

$$m_1 = \sqrt{\frac{p_1 p_2}{p_3 p_4}}, \; m_2 = \frac{p_5}{p_6} m_1 \text{ and } m_3 = \frac{p_4}{p_1} m_1 m_2. \tag{20}$$

The quantities $p_1$ to $p_6$ are given by:

$$\left.\begin{aligned} p_1 = \langle f_4\ f_4\rangle,\ \ p_2 = \langle f_3\ f_3\rangle,\ p_3 = -\frac{1}{\pi}\langle f_2\ f_3\ \mathtt{D}f_4\rangle, \\ p_4 = \frac{2}{\pi\kappa^2}\left\langle \frac{\partial^2 f_2}{\partial X \partial Z}\mathtt{D}f_3\ f_4\right\rangle,\ p_5 = -\frac{1}{\delta^2}\left\langle \nabla^4 f_2\ f_2\right\rangle, \\ p_6 = \frac{\delta^2}{\kappa^2}\left\langle \frac{\partial^2 f_3}{\partial X^2}\ f_2\right\rangle \end{aligned}\right\}, \tag{21}$$

where $\mathtt{D}$ refers the $Z$-derivative. The inner product $\langle f\ g\rangle$ of the two functions, $f(X, Z)$ and $g(X, Z)$, is defined as:

$$\langle f(X,Z)\ g(X,Z)\rangle = \int_{Z=-\frac{1}{2}}^{\frac{1}{2}}\int_{X=0}^{\frac{2\pi}{\kappa}} f(X,Z)\ g(X,Z)dXdZ. \tag{22}$$

The other quantities in equations (17)–(19) are $\delta^2 = \kappa^2 + \pi^2$, $\kappa$ is wave number, $r_{hnl} = \dfrac{Ra_{hnl}\kappa^2}{\delta^6}$, scaled Rayleigh number and $f_i$, $i = 1(1)4$, denotes the eigenfunctions and these must satisfy the Helmholtz equation of the longitudinal rolls plan form and hence $f_i$ have been taken as:

$$\left.\begin{aligned} f_1(X,Z) = \sin(\kappa X)\ \mathtt{D}C_f(Z),\ \ f_2(X,Z) = \cos(\kappa X)C_f(Z) \\ f_3(X,Z) = \cos(\kappa X)\sin\left(\pi Z + \frac{\pi}{2}\right),\ \ f_4(Z) = S(Z) + 2S\left(-\frac{1}{2}\right)Z \end{aligned}\right\}. \tag{23}$$

The function $C_f(Z)$ in equation (23) is the Chandrasekhar function [36] which is defined as:

$$C_f(Z) = \frac{\cosh(\mu_1 Z)}{\cosh(\frac{\mu_1}{2})} - \frac{\cos(\mu_1 Z)}{\cos(\frac{\mu_1}{2})}, \quad (\mu_1 = 4.73004074). \tag{24}$$

The term $f_4(Z)$ arises due to the nonlinear term in the heat equation (10) and it must satisfy the condition:

$$f_4(Z) = 0 \text{ and } \mathtt{D}f_4(Z) \neq 0 \text{ at } Z = \pm\frac{1}{2}. \tag{25}$$

Thus, $S(Z)$ in $f_4(Z)$ is taken as:

$$S(Z) = -\pi\int_{Z_2=0}^{Z}\left\{\int_{Z_1=0}^{Z_2} C_f(Z_1)\sin\pi Z_1\ dZ_1\right\}dZ_2. \tag{26}$$

Substituting equations (17)–(19) in equations (11) and (10) and taking the inner product of the resulting equations with $f_1$, $f_3$ and $f_4$, we get the classical Lorenz model for rigid isothermal boundaries:

$$\frac{dA}{d\tau_1} = Pr^* a_1(-A + B), \tag{27}$$

$$\frac{dB}{d\tau_1} = a_1(r^* A - B - AC), \tag{28}$$

$$\frac{dC}{d\tau_1} = a_1(-b^*C + AB), \tag{29}$$

where $\tau_1 = \epsilon^2\tau$, $Pr^* = \frac{p_5}{p_7}Pr_{hnl}$ , $r^* = \frac{p_8\, p_6}{p_2\, p_5}r_{hnl}$ and $b^* = \frac{p_9}{p_1}b$.

The quantities $p_1$ to $p_6$ are defined in equation (21) and $p_7$, $p_8$ and $p_9$ are defined below:

$$p_7 = \langle \nabla^2 f_2 \cdot f_2 \rangle,\ p_8 = \langle f_2 \cdot f_3 \rangle \text{ and } p_9 = -\frac{1}{4\pi}\langle f_4 \cdot \mathtt{D}^2 f_4 \rangle. \tag{30}$$

The Lorenz model (27)–(29) resembles the classical Lorenz model derived by Lorenz (Ref. [37]) for free boundaries. Hence it retains all the features of the classical system, i.e., Hamilton nature, energy conserving property and bounded solution. Further, the Lorenz model (27)–(29) is analytically intractable. To pursue our objective of obtaining an analytical solution we transform the third-order Lorenz model into the first-order Ginzburg–Landau model (see [14,15]). In other words, we project the third-order Lorenz model into the first-order Ginzburg–Landau model. The Ginzburg–Landau model retains the local stability properties of the Lorenz model in the neighborhood of the critical Rayleigh number. Such a reduction is done in the paper using the renormalization group method (Ref. [38]) which produces an envelop solution that serves as a global solution for the Lorenz system (27)–(29) and it satisfies the Lorenz system approximately but uniformly. This approximate solution of the Lorenz system is valid in the vicinity of the onset of convection and that the determination of its validity domain is a subject of further investigation.

### 2.2 Derivation of the Ginzburg–Landau equation from the Lorenz model using the renormalization group method

Renormalization group method is a powerful perturbation method used to reduce the order of the dynamical system (Refs. [38–40] and references therein). The Taylor series expansion is the basis for this method. Let us consider the Taylor series expansion in $\epsilon$, a small amplitude, as follows:

$$V = \epsilon V_1 + \epsilon^2 V_2 + \epsilon^3 V_3 + \cdots, \tag{31}$$

$$r^* = r_0^* + \epsilon^2 r_2^* \tag{32}$$

where $V_i = [A_i, B_i, C_i]^T$, $i = 1, 2, 3, \ldots$

At the various orders of $\epsilon$ we have the following system of equations:

**First-order system:**

$$\left(\frac{d}{d\tau_1} - L_0\right) V_1 = 0, \tag{33}$$

where

$$L_0 = \begin{pmatrix} -a_1\, Pr & -a_1\, Pr & 0 \\ a_1\, r_0^* & -a_1 & 0 \\ 0 & 0 & -a_1\, b^* \end{pmatrix}. \tag{34}$$

By taking the determinant of $L_0$ equal to zero for a non-trivial solution we obtain $r_0^* = 1$. The eigenvalues of (34) are

$$\lambda_1 = 0,\ \lambda_2 = -a_1(1 + \ Pr),\ \lambda_3 = -a_1\ b^*. \tag{35}$$

The corresponding eigenvectors are

$$H_1 = [1,\ 1,\ 0]^T,\ H_2 = [Pr,\ -1,\ 0]^T,\ H_3 = [0,\ 0,\ 1]^T. \tag{36}$$

In the asymptotic state ($\tau_1 \to \infty$) we may take the neutrally stable solution as

$$V_1(\tau_1, t_0) = M(t_0)H_1, \tag{37}$$

where $t_0$ is the initial time and thus the solution is dependent on $t_0$. Solution (37) in terms of its components form may be written as:

$$A_1(\tau_1) = M(t_0),\ B_1(\tau) = M(t_0),\ C_1(\tau_1) = 0. \tag{38}$$

**Second-order system:**

$$\left(\frac{d}{dt} - L_0\right) V_2 = \begin{pmatrix} 0 \\ -a_1\ A_1C_1 \\ a_1\ A_1B_1 \end{pmatrix} = a_1\ M(t_0)^2 H_3. \tag{39}$$

The second-order system yields the solution

$$V_2(\tau_1, t_0) = \frac{M(t_0)^2}{b^*} H_3. \tag{40}$$

In component form equation (40) may be written as:

$$A_2(\tau_1) = 0,\ B_2(\tau_1) = 0,\ C_2(\tau_1) = \frac{M(t_0)^2}{b^*}. \tag{41}$$

**Third-order system:**

$$\begin{aligned} \left(\frac{d}{d\tau} - L_0\right) V_3 &= \begin{pmatrix} 0 \\ -a_1(r_2^* A_1 - A_1C_2) \\ 0 \end{pmatrix} \\ &= \frac{1}{(1 + Pr^*)} \left(r_2^* M(t_0) - \frac{M(t_0)^3}{b^*}\right) (Pr^* H_1 - H_2). \end{aligned} \tag{42}$$

Equation (42) produces the following solution:

$$V_3 = \frac{1}{(1 + Pr^*)} \left(r_2^* M(t_0) - \frac{M(t_0)^3}{b^*}\right) \left\{a_1\ Pr^*(\tau_1 - t_0)U_1 + \frac{Pr^* H_1 - H_2}{a_1(1 + Pr^*)}\right\}. \tag{43}$$

Thus the perturbation solution of the Lorenz system of equations (27)–(29) around $\tau_1 = t_0$ is

$$V(\tau_1;t_0) = \epsilon M(t_0)H_1 + \epsilon^2\frac{M(t_0)^2}{b^*}H_3 + \frac{\epsilon^3}{(1+Pr^*)}\left[r_2^*M(t_0) - \frac{1}{b^*}M(t_0)^3\right] \times \left\{a_1\ Pr^*(\tau_1 - t_0)H_1 + \frac{Pr^*H_1 - H_2}{a_1(1+Pr^*)}\right\}. \tag{44}$$

Let us now construct the envelope function, $V(\tau_1)$, of the family of trajectories given by the functions $V(\tau_1;t_0,M(t_0))$ with $t_0$ parametrizing the trajectories. In order to construct the envelope function we first impose the following equation:

$$\left.\frac{dV}{dt_0}\right|_{t_0=\tau_1} = 0. \tag{45}$$

Thus using (45), the solution (44) is written as

$$\epsilon\frac{dM}{d\tau_1}H_1 + \frac{2\epsilon^2 M}{b^*}\frac{dM}{d\tau_1}H_3 - \frac{\epsilon^3}{(1+Pr^*)}\left(r_2^*M - \frac{1}{b^*}M^3\right)H_1 = 0. \tag{46}$$

The equation (46) is consistent with $\dfrac{dM}{d\tau_1} = O(\epsilon^2)$. Thus we get the amplitude equation:

$$\frac{dM}{d\tau_1} = \frac{\epsilon^2 a_1\ Pr^*}{1+Pr^*}\left(r_2^*M - \frac{1}{b^*}M^3\right). \tag{47}$$

Using equation (47) we obtain the envelop function:

$$\begin{aligned} V(\tau_1) &= V(\tau_1;\tau_1 = t_0) \\ &= \epsilon M(\tau_1)H_1 + \epsilon^2\frac{M(\tau_1)^2}{b^*}H_3 + \frac{\epsilon^3}{a_1(1+Pr^*)^2}\left[r_2^*M(\tau_1) - \frac{1}{b^*}M(\tau_1)^3\right] \\ &\quad \times (Pr^*H_1 - H_2). \end{aligned} \tag{48}$$

Equation (48) in terms of its components is

$$A(\tau_1) = \epsilon M(\tau_1), \tag{49}$$

$$B(\tau_1) = \epsilon M(\tau_1) + \frac{\epsilon^3}{a_1(1+Pr^*)}\left[r_2^*M(\tau_1) - \frac{1}{b^*}M(\tau_1)^3\right], \tag{50}$$

$$C(\tau_1) = \epsilon^2\frac{M(\tau_1)^2}{b^*}. \tag{51}$$

Substituting equation (49) in the amplitude equation (46) and using equations (31), (38) and (41), we arrive at the Ginzburg–Landau amplitude equation:

$$\frac{dA}{d\tau_1} = \frac{a_1 Pr^*}{(1+Pr^*)}\left[(r^*-1)A - \frac{1}{b^*}A^3\right]. \tag{52}$$

The solution (49)–(51) serves as the local solution of the Lorenz system (27)–(29) and it satisfies the system approximately but uniformly for all values of $\tau_1$ up to

$o(\epsilon^4)$. It is to be also noted here that the solution (49)–(51) is a slow manifold which may identify with a center manifold (Ref. [41]).

Solving equation (52) subject to the initial condition, $A(0) = 1$, we get

$$A(\tau_1) = \frac{\sqrt{Q_1}}{\sqrt{Q_2(1 - e^{-2Q_1\tau_1}) + Q_1 e^{-2Q_1\tau_1}}}, \tag{53}$$

where

$$Q_1 = \frac{a_1\ Pr^*(r^* - 1)}{(1 + Pr^*)} \text{ and } Q_2 = \frac{a_1\ Pr^*}{b^*(1 + Pr^*)}.$$

It is clear from equation (53) that for steady flow

$$A(\infty) = \sqrt{\frac{Q_1}{Q_2}}. \tag{54}$$

Using the steady solution (54) of the Ginzburg–Landau equation (52) obtained from the renormalization group method, in the next section we discuss about the relative coefficient of friction at a particular point on the lower boundary, $Z = -\frac{1}{2}$.

### 2.3 Relative coefficient of friction at the lower plate for a steady flow

The relative coefficient of friction, $\mathscr{C}_f$, is defined as:

$$\mathscr{C}_f = \frac{\text{Coefficient of friction of hybrid nanoliquids}}{\text{Coefficient of friction of baseliquids}}. \tag{55}$$

By having a look at the Figure 1, we arrived at the decision that on the lower plate, $z = -\frac{h}{2}$, the point where $\mathscr{C}_f$ can be calculated is either at $x = \frac{\pi h}{2\kappa_c}$ (the point on the clockwise Rayleigh–Bénard cell touching the lower plate) or the corresponding point $x = \frac{3\pi h}{2\kappa_c}$ on the counter-clockwise cell. It suffices to take one point and so we decide upon $\left(\frac{\pi h}{2\kappa_c}, -\frac{h}{2}\right)$ to evaluate $\mathscr{C}_f$ and this point in nondimensional form written as $\left(\frac{\pi}{2\kappa_c}, -\frac{1}{2}\right)$. The relative coefficient of friction for the Rayleigh–Bénard convection problem is written as:

$$\mathscr{C}_f = \left[\frac{\left(\frac{\partial U}{\partial Z} + \frac{\partial W}{\partial X}\right)_{hnl}}{\left(\frac{\partial U}{\partial Z} + \frac{\partial W}{\partial X}\right)_{bl}}\right]_{\left(\frac{\pi}{2\kappa_c}, -\frac{1}{2}\right)} = a_1. \tag{56}$$

In what follows we use the unsteady solution (53) of the Ginzburg–Landau equation obtained from the renormalization group method to estimate the heat transport

in terms of the Nusselt number at the boundary, $Z = -\frac{1}{2}$, within a wave-length distance in the horizontal direction.

## 3 Enhanced heat transfer in water due to synergising effect of copper and alumina nanoparticles

The thermal Nusselt number, $Nu_{hnl}$, is used to quantify the heat transport and is defined as:

$$Nu_{hnl}(\tau_1) = \frac{\text{Heat transport by (conduction + convection)}}{\text{Heat transport by conduction}}, = 1 + \frac{k_{hnl}}{k_{bl}} \left[ \frac{\int_0^{\frac{2\pi}{\kappa_c}} \left( \frac{\partial \Theta}{\partial Z} \right) dX}{\int_0^{\frac{2\pi}{\kappa_c}} \left( \frac{d\Theta_b}{dZ} \right) dX} \right]_{Z=-\frac{1}{2}}. \tag{57}$$

Substituting equations (7), (19), (40) and (44) and completing integration, we get

$$Nu_{hnl}(\tau_1) = 1 + \left( \frac{k_{hnl}}{k_{bl}} \right) \frac{m_3\, m_4 \kappa_c}{2\pi^2 b^*} \begin{pmatrix} p_8 & p_6 \\ p_2 & p_5 \end{pmatrix} \left( 1 - \frac{1}{r_{hnl}} \right) A^2, \tag{58}$$

where $m_4 = -\frac{2\pi}{\kappa_c} \mathtt{D} f_4 \left( -\frac{1}{2} \right)$.

Using equation (58) we study the heat transport in water-$Al_2O_3$−Cu hybrid nanoliquids. We also compare the influence of a dilute concentration of $Al_2O_3$−Cu and $Al_2O_3$ on the heat transport in water for both rigid isothermal and free isothermal boundaries. A relative Nusselt number, $Nu_r$, of the steady state is needed in the study and the same is defined by:

$$Nu_r^{\infty} = \frac{Nu_{hnl}(\infty)}{Nu(\infty)}. \tag{59}$$

The results of the study and their discussion are presented in the next section.

## 4 Results and discussion

Rayleigh–Bénard convection in water-$Al_2O_3$−Cu hybrid nanoliquid is studied analytically in the paper using the single-phase model proposed by Khanafer et al. [21] but with the thermal conductivity and the viscosity of hybrid nanoliquids obtained from experiment at 300 K (Ref. [26]). The other thermophysical properties of the hybrid nanoliquids are obtained using the traditional mixture theory. The values of thermophysical quantities of water-copper-alumina hybrid nanoliquid, water-alumina nanoliquid, water, copper and alumina are documented in Tables 2–4.

Using the minimal Fourier–Galerkin expansion we arrive at the Lorenz model (27)–(29) for the rigid boundaries. By taking the linear, steady state of version of the

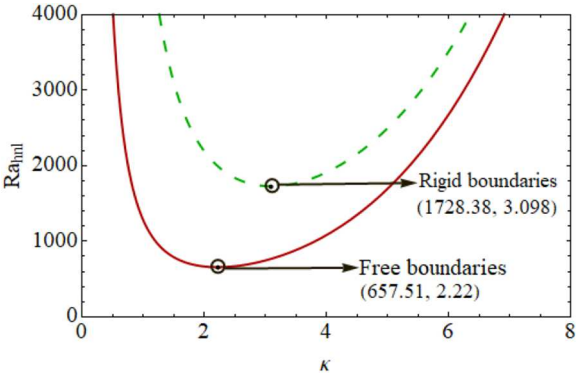


**Fig. 2.** Variation of the Rayleigh number with wave number, $\kappa$, hybrid nanoliquids for free and rigid boundaries.

Lorenz model (27)–(29), we get $r^* = 1$, which indeed means:

$$Ra_{hnl} = \left(\frac{p_2 p_5}{p_8 p_6}\right) \frac{\delta^6}{\kappa^2}. \tag{60}$$

For free isothermal boundaries the above expression is

$$Ra_{hnl}^{FI} = \frac{\delta^6}{\kappa^2}. \tag{61}$$

Figure 2 is the plot of the Rayleigh number versus wave number for rigid and free isothermal boundaries. It is clear from the figure that $Ra_{hnl_c}^{RI} = 2.62867 Ra_{hnl_c}^{FI}$, where the superscripts, $RI$ and $FI$, denote rigid isothermal and free isothermal boundaries. In order to bring in the hybrid nanoliquid effect in the Rayleigh number expression we may write:

$$Ra_{hnl} = F_1 Ra_{bl}, \tag{62}$$

where

$$F_1 = \left(\frac{\rho_{hnl}\ \alpha_{bl}\ \mu_{bl}}{\rho_{bl}\ \alpha_{hnl}\ \mu_{hnl}}\right) \text{ and } Ra_{bl} = \frac{\rho_{bl}\beta_{bl} g \Delta T h^3}{\mu_{bl}\alpha_{bl}}.$$

From Table 5 it is evident that for all values of $\phi_{hnp}$ the factor $F_1$ is less than 1 and as we increase the volume fraction of $Al_2O_3$−Cu in water the value of $F_1$ decreases and this means that the effect of $Al_2O_3$−Cu hybrid nanoparticles in water is to decrease the critical Rayleigh number which in turn implies advancement in the onset of convection. In order to compare the performance of $Al_2O_3$−Cu hybrid nanoparticles with a single nanoparticle ($Al_2O_3$) we have also documented the value of the factor, $F_2 = \left(\frac{\rho_{nl}\ \alpha_{bl}\ \mu_{bl}}{\rho_{bl}\ \alpha_{nl}\ \mu_{nl}}\right)$ for water-$Al_2O_3$ nanoliquids in Table 5. From the table it is evident that $F_1 < F_2$ and this leads to the result:

$$Ra_{hnl_c} < Ra_{nl_c} < Ra_{bl_c}. \tag{63}$$

Equation (63) is true for both rigid isothermal and free isothermal boundaries.

**Table 5.** Values of $F_1$ and $F_2$ for different values of volume fractions of $Al_2O_3-Cu$ hybrid nanoparticles and $Al_2O_3$ nanoparticles.

| $Al_2O_3-Cu$ hybrid nanoparticles volume fraction in % | | | $F_1$ | $Al_2O_3$ nanoparticles volume fraction in % | $F_2$ |
|---|---|---|---|---|---|
| $\phi_{hnp}$ | $\phi_{Cu}$ | $\phi_{Al_2O_3}$ | | $\phi_{Al_2O_3}$ | |
| 0.10 | 0.0962 | 0.0038 | 0.911522 | 0.10 | 0.989409 |
| 0.33 | 0.3175 | 0.0125 | 0.790876 | 0.33 | 0.978135 |
| 0.75 | 0.7215 | 0.0285 | 0.606357 | 0.75 | 0.949942 |
| 1.00 | 0.9620 | 0.0380 | 0.516798 | 1.00 | 0.887494 |
| 2.00 | 1.9241 | 0.0759 | 0.405507 | 2.00 | 0.841814 |

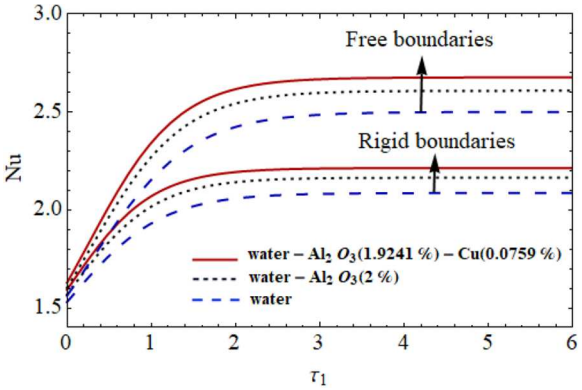


**Fig. 3.** Variation of the Nusselt number with time, $\tau_1$, for water, water-$Al_2O_3$ and water-$Al_2O_3-Cu$ nanoliquids for rigid and free boundaries.

Having analysed some results on the critical Rayleigh number we now present the individual influences of $Al_2O_3-Cu$ hybrid nanoparticles and $Al_2O_3$ nanoparticles on the heat transport in water.

Figure 3 is the plot of Nusselt number, Nu, against time, $\tau_1$, for water-$Al_2O_3-Cu$ hybrid nanoliquid and water-$Al_2O_3$ nanoliquid in the case of both rigid isothermal and free isothermal boundaries. It is clear from this figure that for both rigid isothermal and free isothermal cases the following result is true:

$$Nu_{hnl} > Nu_{nl} > Nu_{bl}. \tag{64}$$

The percentage enhancement, E, in heat transport in water due to presence of $Al_2O_3-Cu$ hybrid nanoparticles and $Al_2O_3$ nanoparticles is reported in Tables 6 and 7, respectively using the information on heat transport in water documented in Table 8. From Table 6 it is clear that the percentage of heat transfer enhancement in water due to $Al_2O_3-Cu$ hybrid nanoparticles increases with increase in volume fraction of $Al_2O_3-Cu$ hybrid nanoparticles. It is shown that for $r_{hnl} = 4$, 2% of $Al_2O_3-Cu$ hybrid nanoparticles in water provides 6.44% heat transfer enhancement in water for rigid isothermal boundaries and 7.65% heat transfer enhancement in water for free isothermal boundaries whereas 2% of $Al_2O_3$ nanoparticles in water provides 4.01% heat transfer enhancement in water for rigid isothermal boundaries and 4.7% heat transfer enhancement in water for free isothermal boundaries. Thus, compared to $Al_2O_3$ nanoparticles, $Al_2O_3-Cu$ hybrid nanoparticles enhance heat transport around 2.43% more for rigid isothermal boundaries and around 2.95% more for free isothermal boundaries.

**Table 6.** Values of Nusselt number for water-$Al_2O_3-Cu$ hybrid nanoliquid for different values of volume fraction of $Al_2O_3-Cu$ hybrid nanoparticles for rigid and free boundaries.

| $Al_2O_3-Cu$ hybrid nanoparticles volume fraction in % | | | Rigid boundaries | | | | Free boundaries | | | |
|---|---|---|---|---|---|---|---|---|---|---|
| $\phi_{hnp}$ | $\phi_{Al_2O_3}$ | $\phi_{Cu}$ | $Nu_{hnl}$ $(r_{hnl}=2)$ | $E$ | $Nu_{hnl}$ $(r_{hnl}=4)$ | $E$ | $Nu_{hnl}$ $(r_{hnl}=2)$ | $E$ | $Nu_{hnl}$ $(r_{hnl}=4)$ | $E$ |
| 0.10 | 0.0962 | 0.0038 | 1.73206 | 0.63 | 2.09809 | 0.78 | 2.00602 | 0.78 | 2.50903 | 0.93 |
| 0.33 | 0.3175 | 0.0125 | 1.74542 | 1.41 | 2.11813 | 1.75 | 2.02519 | 1.74 | 2.53778 | 2.09 |
| 0.75 | 0.7215 | 0.0285 | 1.76725 | 2.68 | 2.15088 | 3.32 | 2.05636 | 3.31 | 2.58454 | 3.97 |
| 1.00 | 0.9620 | 0.0380 | 1.77694 | 3.24 | 2.16540 | 4.02 | 2.07018 | 4.00 | 2.60527 | 4.81 |
| 2.00 | 1.9241 | 0.0759 | 1.81052 | 5.19 | 2.21579 | 6.44 | 2.11725 | 6.37 | 2.67587 | 7.65 |

**Table 7.** Values of Nusselt number for water-$Al_2O_3$ nanoliquid for different values of volume fraction of $Al_2O_3$ nanoparticles for rigid and free boundaries.

| $Al_2O_3$ nanoparticles volume fraction in % ($\phi_{Al_2O_3}$) | Rigid boundaries | | | | Free boundaries | | | |
|---|---|---|---|---|---|---|---|---|
| | $Nu_{nl}$ $(r_{nl}=2)$ | $E$ | $Nu_{nl}$ $(r_{nl}=4)$ | $E$ | $Nu_{nl}$ $(r_{nl}=2)$ | $E$ | $Nu_{nl}$ $(r_{nl}=4)$ | $E$ |
| 0.10 | 1.72484 | 0.21 | 2.08725 | 0.26 | 1.99556 | 0.25 | 2.49334 | 0.30 |
| 0.33 | 1.73080 | 0.56 | 2.09620 | 0.69 | 2.00390 | 0.67 | 2.50585 | 0.81 |
| 0.75 | 1.74522 | 1.40 | 2.11783 | 1.73 | 2.02409 | 1.69 | 2.53613 | 2.02 |
| 1.00 | 1.76067 | 2.29 | 2.14101 | 2.84 | 2.04590 | 2.78 | 2.56885 | 3.34 |
| 2.00 | 1.77679 | 3.23 | 2.16518 | 4.01 | 2.06844 | 3.91 | 2.60266 | 4.70 |

**Table 8.** Values of Nusselt number for water for rigid and free boundaries.

| Rigid boundaries ($Nu$) | | Free boundaries ($Nu$) | |
|---|---|---|---|
| $r=2$ | $r=4$ | $r=2$ | $r=4$ |
| 1.7212 | 2.0818 | 1.99053 | 2.4858 |

A better understanding with physical explanation of the observed results, can be had by including the plots of the stream function, the isotherms and the coefficient of friction and the same is included as Figures 4–6. Observing the plots of stream function and isotherm in Figures 4 and 5 it can be seen that the $Al_2O_3-Cu$ hybrid nanoparticles intensify convection in water more than the $Al_2O_3$ mono nanoparticles. The reason for this can be extracted by considering these plots in conjunction with the plots of the relative coefficient of friction (6). It is obvious that relative coefficient of friction is more in the case of water-$Al_2O_3-Cu$ compared to water-$Al_2O_3$ and hence the aforementioned result. A similar explanation can be given in the context of the rigid boundary influence on Rayleigh–Bénard convection in nanoliquids and hybrid nanoliquids.

## 5 Conclusion

Suspending new generation (hybrid) nanoparticles in the base liquid is a recent development in nanoliquid heat transfer research. It is thus worth studying theoretically the heat transfer performance in hybrid nanoliquid by Rayleigh–Bénard convection. Since dilute concentrations of nanoliquids were used in such studies the model with single-phase description is a preferred one. If one is looking for stability of the system in addition to heat transfer enhancement in application situation then in those

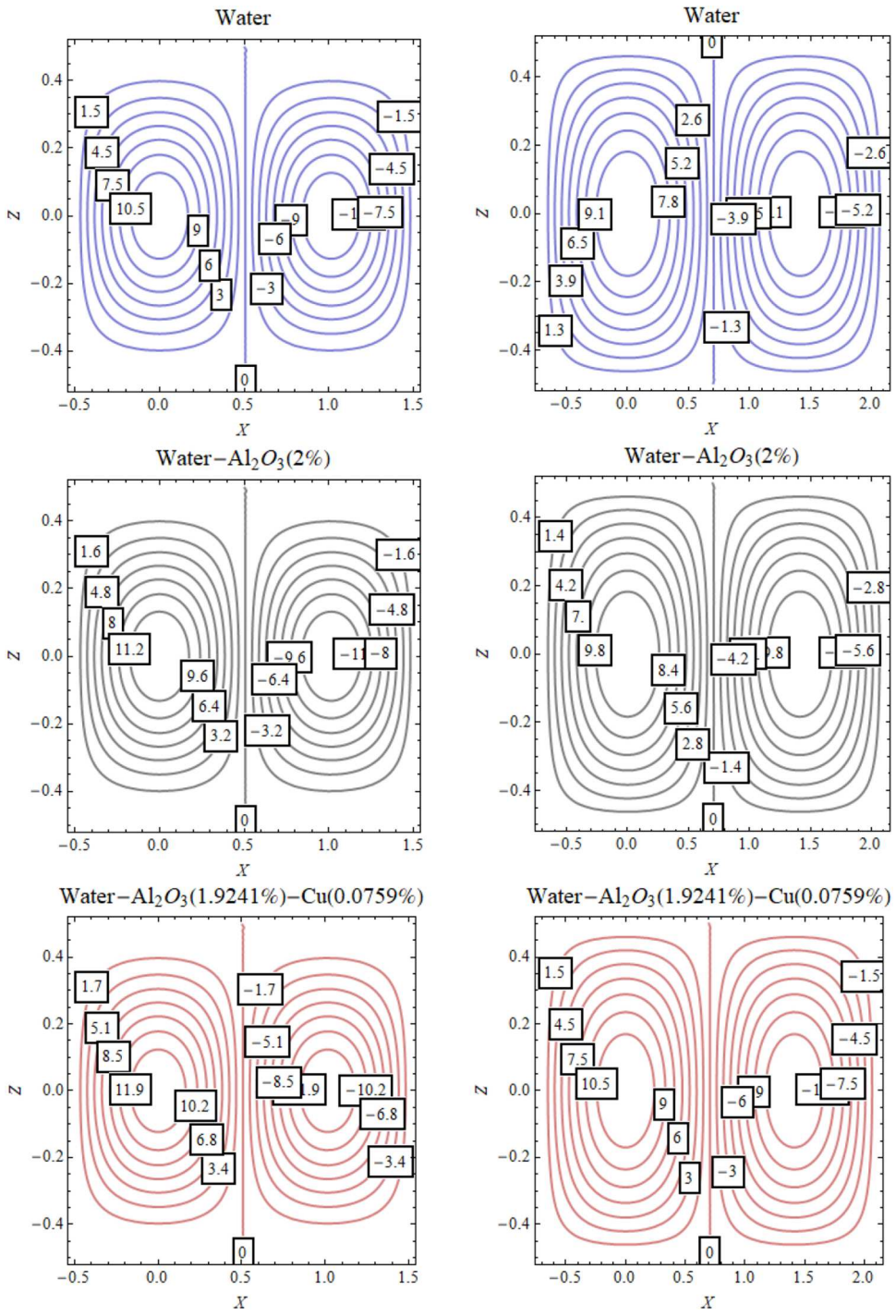


**Fig. 4.** Plot of the streamline for water, water-$Al_2O_3$ and water-$Al_2O_3-Cu$ for both rigid(left) and free(right) boundaries.

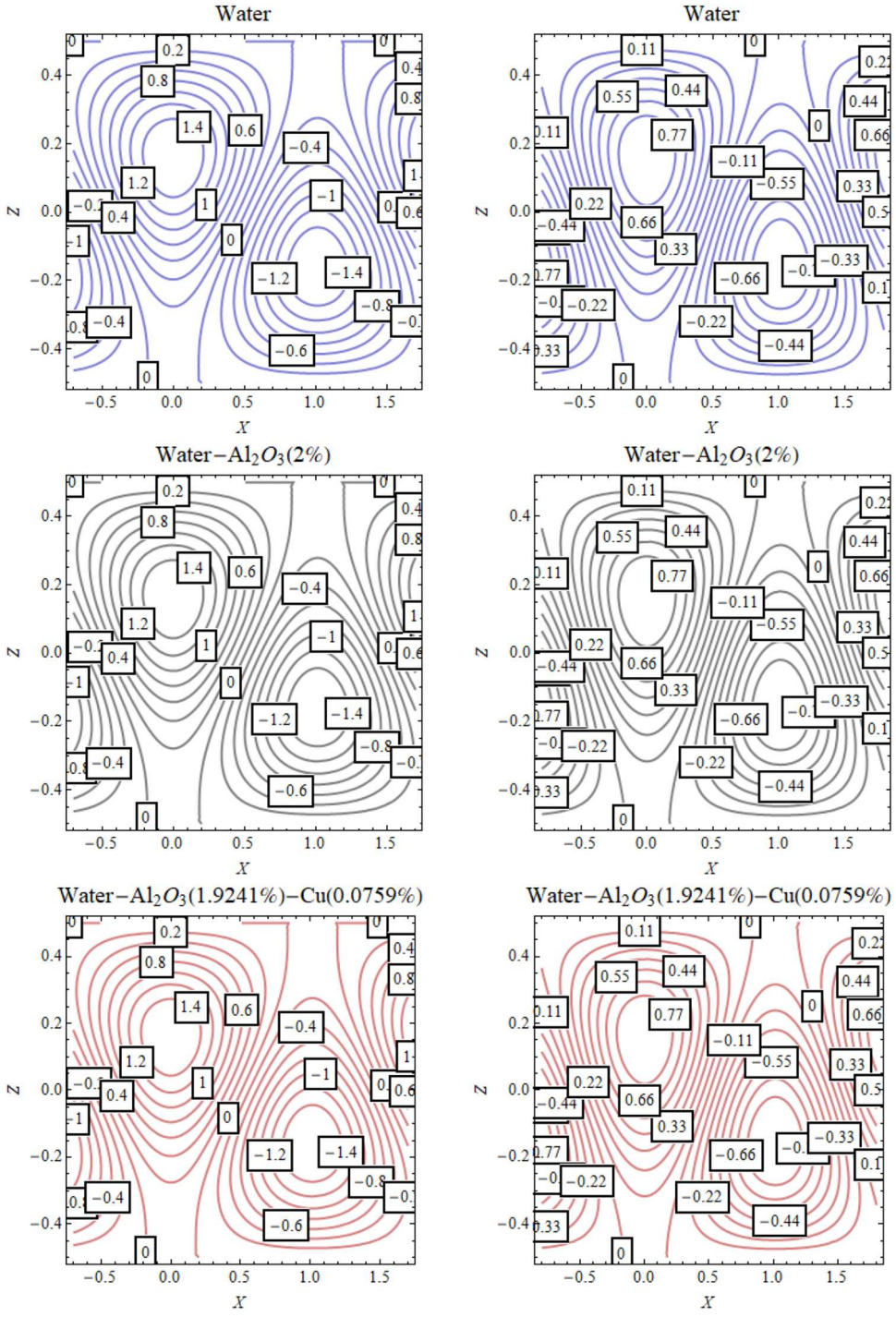


**Fig. 5.** Plot of the isotherms for water, water-$Al_2O_3$ and water-$Al_2O_3-Cu$ for both rigid(left) and free(right) boundaries.

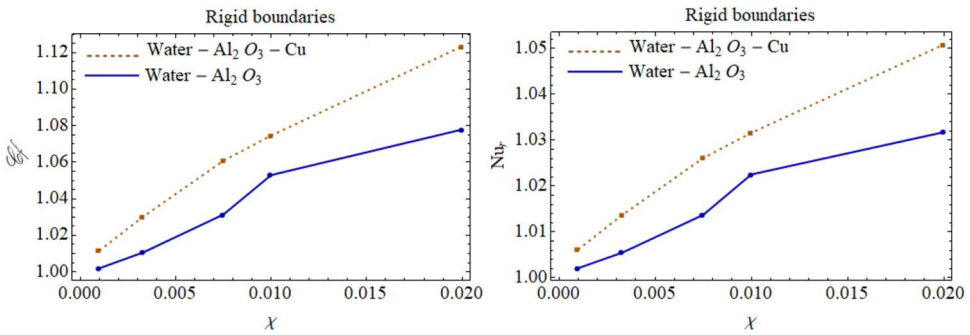


**Fig. 6.** Plot of the relative coefficient of friction, $\mathscr{C}_f$(left), and relative Nusselt number, $Nu_r$(right), versus $\chi$ for water-$Al_2O_3$ and water-$Al_2O_3-$Cu nanoliquids for the case of rigid boundaries.

cases alumina is the best choice of nanoparticles. This is because it is theoretically and experimentally proven that alumina is more stable in liquids compared to many other nanoparticles. The problem with alumina nanoparticle, however, is that it is has very less thermal conductivity than other nanoparticles (around 10 times less than that of copper nanoparticles). To retain such a stability and also to have maximum heat transfer enhancement one can think of including alumina nanoparticles with small amounts of other nanoparticles which have higher thermal conductivity. While choosing the proportion of alumina and the other nanoparticle one has to take additional care to retain the stability feature of alumina. The present paper is an attempt to provide vital information to those who seek stability as well as best heat transfer performance in the Rayleigh–Bénard convective mechanism. To keep the problem realistic we opted for an experimental or realistic boundary condition, namely, rigid isothermal boundaries. From the present study we arrived at the following general conclusion:

- The error in the estimation of the critical Rayleigh number for rigid isothermal boundaries in the present study when compared with the most accurate value (Ref. [36]) is 1.24%.
- $Ra_c^{RI} = 2.62867\ Ra_c^{FI}$ for all working media.
- $Ra_{w-Al_2O_3-Cu_c} < Ra_{w-Al_2O_{3_c}} < Ra_{w_c}$
  The result is true for both rigid isothermal and free isothermal boundaries.
- $Nu_{w-Al_2O_3-Cu} > Nu_{w-Al_2O_3} > Nu_w$
  The result is true for both rigid isothermal and free isothermal boundaries.
- The percentage enhancement of heat transfer in water due to 2% $Al_2O_3-$Cu hybrid nanoparticles is 6.44% for rigid boundaries and 7.65% for free boundaries.
- The percentage enhancement of heat transfer in water due to 2% $Al_2O_3$ nanoparticles is 4.01% for rigid boundaries and 4.7% for free boundaries.
- The percentage enhancement of heat transfer in water due to 2% of $Al_2O_3-$Cu hybrid nanoparticles compared to 2% of $Al_2O_3$ nanoparticles is 2.43% for rigid boundaries and 2.95% for free boundaries.
- Convection is more intense in the case of water-$Al_2O_3-$Cu nanoliquid compared to that of water-$Al_2O_3$ nanoliquid. This is because $\mathscr{C}_f^{hnl} > \mathscr{C}_f^{nl}$. Thereby we also have $Nu_r^{hnl} > Nu_r^{nl}$.

– The stream function and isotherm plots reiterates the earlier findings.

– The relative coefficient of friction has physical significance in that it can be identified with the ratio of thermal diffusivities, $a_1$.

The authors (KC and YZ) acknowledge Foundation of Guizhou Provincial Key Laboratory of Public Big Data (No. 2018BDKFJJ017) and the National Natural Science Foundation of China (No. 61573119) for financial support and a Fundamental Research Project of Shenzhen under Project Nos. KQJSCX20180328165509766 and JCYJ20170307151312215. The author (PGS) is thankful to Professor Yi Zhao for financial support to visit his research group for collaborative work. The authors would like to thank the reviewer and the Editor for useful comments that helped us to improve the paper.

## Author contribution statement

The author PGS provided the idea, formulation of the problem and finalized the ultimate version of the manuscript. The authors KC and YZ worked on the details of the problem, methodology, presentation and the several drafts of the manuscript. All authors approve the ultimate version for publication.

## References

1. M. Gollin, D. Bjork, SAE Technical Paper, https://doi.org/10.4271/960372 (1996)
2. P.I. Frank, P.D. David, *Fundamentals of heat transfer* (Wiley, New York, 1981)
3. W.M. Yan, P.J. Sheen, Int. J. Heat Mass Transfer **43**, 1651 (2000)
4. C.C. Wang, K.Y. Chi, Int. J. Heat Mass Transfer **43**, 2681 (2000)
5. P. Ravi, Phy. Rev. Lett. **94**, 025901 (2005)
6. H. Masuda, A. Ebata, K. Teramae, Netsu Bussei **4**, 227 (1993)
7. S. Choi, ASME Publications Fed **231**, 99 (1995)
8. J.A. Eastman, S.U.S. Choi, S. Li, W. Yu, L.J. Thompson, Appl. Phys. Lett. **78**, 718 (2001)
9. D.H. Kumar, H.E. Patel, V.R.K. Rajeev, T. Sundararajan, T. Pradeep, S.K. Das, Phys. Rev. Lett. **93**, 144301 (2004)
10. S. Kakac, A. Pramuanjaroenkij, Int. J. Heat Mass Transfer **52**, 3187 (2009)
11. Z. Haddad, H.F. Oztop, E. Abu-Nada, A. Mataoui, Renew. Sustain. Energy Rev. **16**, 5363 (2012)
12. P.G. Siddheshwar, C. Kanchana, Int. J. Mech. Sci. **131–132**, 1061 (2017)
13. C. Kanchana, Y. Zhao, Int. J. Heat Mass Transfer **127**, 1031 (2018)
14. C. Kanchana, Y. Zhao, P.G. Siddheshwar, Phys. Fluids **30**, 084101 (2018)
15. P.G. Siddheshwar, C. Kanchana, Meccanica **54**, 451 (2019)
16. H.A. Mintsa, G. Roy, C.T. Nguyen, D. Doucet, Int. J. Therm. Sci. **48**, 363 (2009)
17. J. Buongiorno, ASME J. Heat Transfer **128**, 240 (2006)
18. P.G. Siddheshwar, C. Kanchana, Y. Kakimoto, A. Nakayama, ASME J. Heat Transfer **139**, 012402 (2016)
19. P.G. Siddheshwar, K.M. Lakshmi, ASME J. Heat Transfer **141**, 062405 (2019)
20. F. Garoosi, G. Bagheri, M.M. Rashidi, Powder Technol. **275**, 239 (2015)
21. K. Khanafer, K. Vafai, M. Lightstone, Int. J. Heat Mass Transfer **46**, 3639 (2003)
22. R.Y. Jou, S.C. Tzeng, Int. Commun. Heat Mass Transfer **33**, 727 (2006)
23. P.G. Siddheshwar, N. Meenakshi, Int. J. Appl. Comput. Math. **3**, 271 (2017)
24. C. Simó, D. Puigjaner, J. Herrero, F. Giralt, Commun. Nonlinear Sci. Numer. Simul. **15**, 24 (2010)
25. J. Jawdat, I. Hashim, S. Momani, Math. Probl. Eng. **2012**, 1 (2012)

26. S. Suresh, K. Venkitaraj, P. Selvakumar, M. Chandrasekar, Colloids Surf. A: Physicochem. Eng. Asp. **388**, 41 (2011)
27. S. Suresh, K. Venkitaraj, P. Selvakumar, M. Chandrasekar, Exp. Therm. Fluid Sci. **38**, 54 (2012)
28. F. Selimefendigil, A.J. Chamkha, Comput. Therm. Sci. **8**, 555 (2016)
29. T. Hayat, S. Nadeem, Results Phys. **7**, 2317 (2017)
30. K.A. Hamid, W.H. Azmi, M.F. Nabil, R. Mamat, IOP Conf. Series: Mater. Sci. Eng. **257**, 012067 (2017)
31. L.S. Sundar, K.V. Sarma, M.K. Singh, A.C.M. Sousa, Renew. Sustain. Energy Rev. **68**, 185 (2017)
32. W.F. Nabil, W.H. Azmi, K.A. Hamid, N.N.M. Zawawi, G. Priyandoka, R. Mamat, Int. Commun. Heat Mass Transfer **83**, 30 (2017)
33. N. Ali, J.A. Teixeira, A. Addali1, J. Nanomater. **2018**, 1 (2018)
34. M. Izadi, R. Mohebbi, D. Karimi, M.A. Sheremet, Chem. Eng. Process.: Process Intensif. **125**, 56 (2018)
35. M.H. Esfe, S. Wongwises, A. Naderi, A. Asadi, M.R. Safaei, H. Rostamian, M. Dahari, A. Karimipour, Int. Commun. Heat Mass Transfer **66**, 100 (2015)
36. S. Chandrasekhar, *Hydrodynamic and hydromagnetic stability* (Oxford University Press, New York, 1961)
37. E.N. Lorenz, J. Atmos. Sci. **20**, 130 (1963)
38. T. Kunihiro, Prog. Theor. Phy. **97**, 179 (1997)
39. N. Goldenfeld, *Lectures on phase transitions and the renormalization group* (Addison Wesley, Reading, Massachusetts, 1992)
40. L.Y. Chen, N. Goldenfeld, Y. Oono, Phy. Rev. Lett. **73**, 1311 (1994)
41. P.G. Siddheshwar, in *Proceedings of International Conference on Mathematical Modeling in Science and Engineering, 2019*, p. 46